THE ASTROPHYSICAL JOURNAL, 428:L33–L36, 1994 June 10

DISCOVERY OF $^{14}NH_3(3, 3)$ MASER EMISSION IN THE INTERSTELLAR MEDIUM

JEFFREY G. MANGUM
Submillimeter Telescope Observatory, Steward Observatory, University of Arizona, Tucson, AZ 85721

AND

ALWYN WOOTTEN
National Radio Astronomy Observatory,[1] 520 Edgemont Road, Charlottesville, VA 22903
Received 1994 February 3; accepted 1994 March 25

ABSTRACT

We report the discovery of $^{14}NH_3(3, 3)$ maser emission toward the DR 21(OH) star-forming region. This maser emission is spatially and spectrally coincident with CH_3OH maser emission. Given the position of these $^{14}NH_3$ and CH_3OH masers relative to the observed outflow emission in DR 21(OH), along with the recent observation that thermal $^{14}NH_3(3, 3)$ emission traces outflows, we conclude that $^{14}NH_3$ and CH_3OH masers are produced within shocked molecular outflows. The sensitivity of the $^{14}NH_3(3, 3)$ maser emission to the ortho-H_2/para-H_2 ratio has allowed us to derive an upper limit of 10^6 yr to the age of the cloud which gives rise to the $^{14}NH_3(3, 3)$ maser emission.

Subject headings: ISM: clouds — ISM: individual [DR 21(OH)] — ISM: molecules — masers — molecular data — molecular processes — radio lines: ISM

1. INTRODUCTION

Ammonia ($^{14}NH_3$: in the following we will denote $^{14}NH_3$ by NH_3) masers have been a topic of great interest in the study of star formation for a number of years. Early measurements of the metastable (3, 3) inversion transition toward the W33 (Wilson, Batrla, & Pauls 1982), DR 21 (Guilloteau et al. 1983), and W28 A2 (Gómez et al. 1991) star-forming regions indicated possible inversion of this transition. Unfortunately, high spatial resolution VLA measurements of the $NH_3(3, 3)$ emission toward DR 21 failed to detect maser emission and indicated that the (3, 3) emission detected with low spatial resolution was due to an extended ($\theta_s \gtrsim 10''$), low surface brightness region. It was not until measurements of the ^{15}N isotopomer of NH_3, $^{15}NH_3$, were made that masing in the (3, 3) inversion transition was confirmed (Mauersberger, Wilson, & Henkel 1986; Johnston et al. 1989). Subsequently, discoveries of maser emission in highly excited nonmetastable states of NH_3 (Madden et al. 1986; Wilson & Henkel 1988; Mauersberger, Henkel, & Wilson 1987; Mauersberger, Wilson, & Henkel 1988) were made. Recently, maser emission in the metastable (5, 5) transition of NH_3 has been detected toward the G9.26+0.19 molecular cloud (Cesaroni, Walmsley, & Churchwell 1992).

In general, the pumping mechanism for the ammonia masers is not well understood. Models of the collisional excitation of NH_3 indicate that population inversions of the (3, 3) transition are collisionally induced (Flower, Offer, & Schilke 1990). Pumping in the nonmetastable states of NH_3 is not currently understood. Possible pump mechanisms include an interaction with infrared vibrational lines (Brown & Cragg 1987; Mauersberger et al. 1987) and line overlap with infrared lines from other molecules such as H_2O (Madden et al. 1986).

In this *Letter* we report the discovery of $NH_3(3, 3)$ maser emission toward the active star formation region DR 21(OH). This represents the first confirmed detection of $NH_3(3, 3)$ maser emission in the interstellar medium.

2. OBSERVATIONS

Observations of the $NH_3(3, 3)$ transition were made during two separate observing runs on 1991 April 14 and 1992 April 14 using the NRAO Very Large Array. The 27 antennas were in the D configuration during the 1991 observations, while for the 1992 observations the antennas were in the C configuration. Identical observational parameters were used for both observing runs. Sixty-four spectral channels were used to sample the 1.5625 MHz intermediate frequency bandwidth, which, after on-line Hanning smoothing, resulted in a frequency resolution and channel spacing of 24.414 kHz. At the $NH_3(3, 3)$ transition rest frequency of 23.870129610 GHz this channel spacing yielded a velocity resolution of 0.307 km s^{-1} and a velocity coverage of 19.624 km s^{-1} centered at an LSR velocity of -3.0 km s^{-1}. DR 21(OH) was observed with an antenna pointing position of $\alpha(1950) = 20^h37^m14^s.0$, $\delta(1950) = 42°12'00''$. The phase calibration source was 2005+403 (measured flux density 2.52 Jy [1991] and 2.24 Jy [1992]). To establish the flux density scale, an observation of 3C 286 (assumed flux density 2.43 Jy) was made. The accuracy of the flux density calibration is $\sim 10\%$.

An observation of 3C 273 (measured flux density 40.00 Jy) was used to calibrate the bandpass during the 1991 observations, while a measurement of 3C 84 (measured flux density 24.15 Jy) was used during the 1992 observations. Calibration of the individual antenna amplitudes and phases was obtained using the AIPS program.

The strong continuum source DR 21 is located 180″ south of our antenna pointing position, placing it near the first null of the antenna primary beam (FWHM = 1′.9). The emission from this source produces map distortions within the region of interest in both *u-v* data sets. Removal of these distortions was accomplished by constructing a model of DR 21 for each *u-v* data set using the CLEAN algorithm in AIPS. This CLEAN model was then subtracted from each *u-v* data set, resulting in a great improvement in map fidelity.

[1] The National Radio Astronomy Observatory is operated by Associated Universities, Inc., under cooperative agreement with the National Science Foundation.

Before merging the C- and D-array u-v data sets, we compared their u-v flux intensities. We found that the absolute flux scale of the two data sets agrees to within 10%. The AIPS task DBCON was then used to merge the individual C- and D-array u-v data sets.

To extract DR 21(OH) source continuum emission from our u-v data, channels on both ends of our observed bandpass which were determined to be free of $NH_3(3, 3)$ line emission were imaged to produce two independent continuum maps. Inspection of the dirty channel images of the entire u-v data set and the single-antenna $NH_3(3, 3)$ measurements from Wilson & Mauersberger (1990) indicates that for 4.0 km s^{-1} $\leq V_{LSR} \leq$ 5.6 km s^{-1} and -11.0 km s^{-1} $\leq V_{LSR} \leq -9.1$ km s^{-1} our channel maps are free of line emission and are far enough away from the band edges to produce good line-free images. The two dirty images produced from these velocity ranges, which were quite similar in overall structure and intensity, were then combined and CLEANed. This CLEAN model was then subtracted from the entire u-v data set, which resulted in a single u-v data set which contained only $NH_3(3, 3)$ emission.

CLEAN maps of our C- and D-array continuum-free data set were made. With natural weighting of the visibilities, the resulting beam size was 2.″80 × 2.″69 at a position angle of $-77°$. The rms noise was 3.5 mJy beam^{-1} (15.1 K) in each of the resultant 0.3 km s^{-1} wide velocity channels. By using only u-v spacings greater than 50 kλ and applying a uniform weighting to the visibilities, we were able to emphasize the small-scale structure in the data. The resulting synthesized beam size was 0.″73 × 0.″68 at a position angle of 31°.

3. RESULTS AND ANALYSIS

3.1. *Properties of the Western* $NH_3(3, 3)$ *Emission Source*

In Figure 1 we show the velocity-integrated intensity image of the DR 21(OH) main region from our $NH_3(3, 3)$ data set. On this image we indicate the positions for the OH (Norris et al. 1982), H_2O (Mangum, Wootten, & Mundy 1992), and CH_3OH (Plambeck & Menten 1990) masers of the region along with the 1.4 mm (Woody et al. 1989), 2.7 mm (Mangum, Wootten, & Mundy 1991), 1.2 cm (Mangum & Wootten 1994), and 2.1 cm (Mangum & Wootten 1994) continuum, H_2CO $2_{11} \rightarrow 2_{12}$ (Mangum & Wootten 1994), and $NH_3(1, 1)$ and $NH_3(2, 2)$ (Mangum et al. 1992) emission peaks. The strong $NH_3(3, 3)$ emission peak located on the west side of the emission distribution, which is coincident with CH_3OH maser 1, has no corresponding $NH_3(1, 1)$, $NH_3(2, 2)$, or $NH_3(4, 4)$ emission (Mangum et al. 1992; Mangum & Wootten 1994). The results from a Gaussian fit to the peak channel for this $NH_3(3, 3)$ emission component are shown in Table 1. Also in Figure 1 we present a spectrum taken through the peak position of this emission feature and compare it with published CH_3OH maser emission spectra at this same position. Given that this $NH_3(3, 3)$ emission feature is unresolved ($\theta_{min} < \theta_{beam}$), has a large brightness temperature (peak $T_B \gtrsim 1127$ K), and a narrow line width ($\Delta v_{FWZI} \simeq 1.2$ km s^{-1}), it appears that it is an $NH_3(3, 3)$ maser.

TABLE 1

$NH_3(3, 3)$ MASER PROPERTIES[a]

Parameter	Value
α(1950)	$20^h37^m12^s.35$
δ(1950)	42°12′11.″1
V_{LSR} (km s^{-1})	0.37
Δv_{FWZI} (km s^{-1})	1.2
θ_{maj}	0.″99
θ_{min}	0.″59
Position angle	8°.2
S_ν^{peak} (mJy beam^{-1})	260.4 ± 1.5
T_B^{peak} (K)	1127[b]

[a] As derived from our 0.″73 × 0.″68 resolution data set.

[b] Note that since the source is unresolved, this brightness temperature is a lower limit.

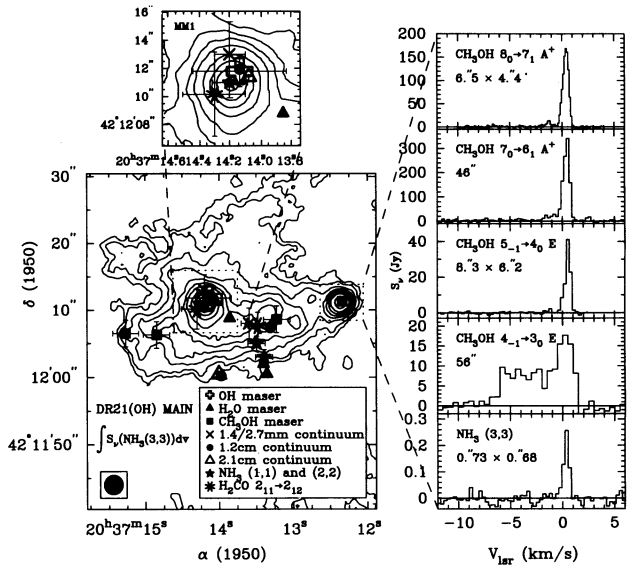

FIG. 1.—$NH_3(3, 3)$ emission toward DR 21(OH) main. The contours are velocity-integrated $NH_3(3, 3)$ intensity in units of 2, 4, 8, 12, 16, 20, 25, 35, 45, 55, and 65 times the rms noise of 7.0 mJy beam^{-1} km s^{-1} in this image. The positions of the OH (Norris et al. 1982), H_2O (Mangum, Wootten, & Mundy 1992), and CH_3OH masers (Plambeck & Menten 1990), the 1.4 mm (Woody et al. 1989), 2.7 mm (Mangum, Wootten, & Mundy 1991), 1.2 cm (Mangum & Wootten 1994), and 2.1 cm (Mangum & Wootten 1994) continuum sources, and the $NH_3(1, 1)$ and $NH_3(2, 2)$ (Mangum, Wootten, & Mundy 1992) and H_2CO $2_{11} \rightarrow 2_{12}$ (Mangum & Wootten 1994) emission sources are indicated using the symbols shown. The uncertainties for these positions are taken either from the source of the position (OH, H_2O, and CH_3OH masers), from the uncertainties resultant from Gaussian fits to the data (1.2 and 2.1 cm continuum), from the amount of wandering in velocity that a source does for spectral line measurements [$NH_3(1, 1)$ and $NH_3(2, 2)$ and H_2CO $2_{11} \rightarrow 2_{12}$ emission), or by assuming one-third of a beam (1.4 and 2.7 mm continuum). The upper inset details a close-up view of the DR 21(OH) MM 1 region. The spectral inset of the western $NH_3(3, 3)$ source, drawn from our high spatial resolution data set, is a comparison between the $NH_3(3, 3)$ maser emission and the CH_3OH maser emission toward this position. The references for the CH_3OH maser spectra are Haschick & Baan (1989) ($4_{-1} \rightarrow 3_0$ E), Batrla & Menten (1988) ($5_{-1} \rightarrow 4_0$ E); Haschick, Menten, & Baan (1990) ($7_0 \rightarrow 6_1$ A^+); and Plambeck & Menten (1990) ($8_0 \rightarrow 7_1$ A^+). The beam sizes used for each measurement are shown.

In order for a transition to produce maser emission, the energy levels which give rise to the emission must possess an inverted population distribution. This population inversion leads to a negative transition excitation temperature and optical depth. To show that indeed the $NH_3(3, 3)$ transition can produce maser emission, we have constructed large velocity gradient (LVG) models of the ortho-NH_3 excitation. Using the collisional excitation rates of Danby et al. (1988), we have made model predictions of the $NH_3(3, 3)$ brightness temperature and optical depth for kinetic temperature T_K = 10–300 K, $n(H_2) = 10^3$–10^9 cm^{-3}, and $N(\text{ortho-}NH_3)/\Delta v = 10^{13}$–$10^{17}$ cm^{-2} (km s^{-1})$^{-1}$. A sample of the LVG model

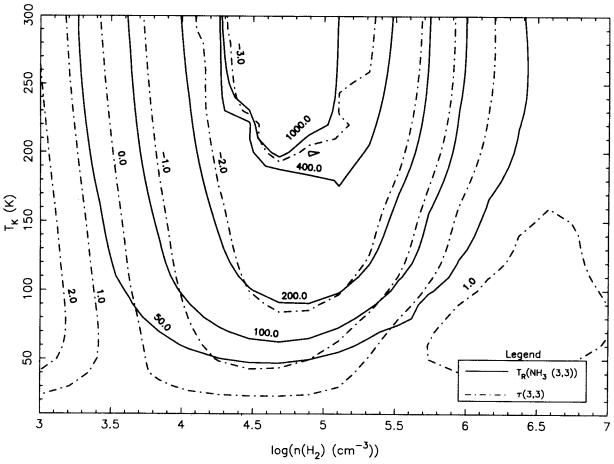

FIG. 2.—$NH_3(3, 3)$ LVG model predictions. Shown are the contours of $NH_3(3, 3)$ radiation temperature [$T_R(NH_3(3, 3))$] in K and $NH_3(3, 3)$ optical depth [$\tau(3, 3)$] at log [$N(\text{ortho-}NH_3)/\Delta v$] = 15 cm^{-2} (km $s^{-1})^{-1}$.

predictions is shown in Figure 2. Note that when we refer to H_2 we assume that all H_2 is in its ground state (para) form. This region of [T_K, $n(H_2)$, $N(\text{ortho-}NH_3)/\Delta v$] parameter space was chosen to span that found in most molecular cloud cores. The LVG models predict that the $NH_3(3, 3)$ transition possesses $\tau(3, 3) < 0$ for $T_K > 20$ K, $10^{3.5}$ $cm^{-3} < n(H_2) < 10^{7.3}$ cm^{-3}, and $N(\text{ortho-}NH_3)/\Delta v < 10^{16.8}$ cm^{-2} (km $s^{-1})^{-1}$. $T_B(3, 3) \gtrsim 1127$ K requires $T_K > 100$ K, $10^{3.4}$ $cm^{-3} < n(H_2) < 10^5$ cm^{-3}, and $N(\text{ortho-}NH_3)/\Delta v > 10^{14.8}$ cm^{-2} (km $s^{-1})^{-1}$. Therefore, in order to produce the combined effect of $\tau(3, 3) < 0$ *and* $T_B(3, 3) \gtrsim 1127$ K, the gas must have $T_K > 100$ K, $10^{3.4}$ $cm^{-3} < n(H_2) < 10^5$ cm^{-3}, and $10^{14.8}$ cm^{-2} (km $s^{-1})^{-1} < N(\text{ortho-}NH_3)/\Delta v < 10^{16.8}$ cm^{-2} (km $s^{-1})^{-1}$. To produce $T_B(3, 3) \gtrsim 1127$ K but *without* maser emission [$\tau(3, 3) > 0$] requires $T_K > 100$ K, $10^{3.4}$ $cm^{-3} < n(H_2) < 10^5$ cm^{-3}, and $N(\text{ortho-}NH_3)/\Delta v > 10^{16.8}$ cm^{-2} (km $s^{-1})^{-1}$.

As noted above, no $NH_3(1, 1)$, $NH_3(2, 2)$, or $NH_3(4, 4)$ emission is detected toward the western $NH_3(3, 3)$ source. Using the 2 σ limits from our $NH_3(1, 1)$, $NH_3(2, 2)$, and $NH_3(4, 4)$ measurements in combination with our LVG models, we find that nondetections of these transitions require $N(\text{ortho-}NH_3)/\Delta v \lesssim 10^{16}$ cm^{-2} (km $s^{-1})^{-1}$. Note also that $N(\text{ortho-}NH_3)/\Delta v \lesssim 10^{16.7}$ cm^{-2} (km $s^{-1})^{-1}$ within the subcondensations of the Orion-KL hot core component (Hermsen, Wilson, & Bieging 1988). Since the Orion-KL hot core component is in itself unusual in that it possesses an NH_3 abundance which is approximately 10^3 times that measured toward most molecular clouds (Irvine et al. 1985; Blake et al. 1987), we conclude that model solutions with $N(\text{ortho-}NH_3)/\Delta v > 10^{16.8}$ cm^{-2} (km $s^{-1})^{-1}$ do not accurately describe the true physical properties of the $NH_3(3, 3)$ source under study. Therefore, the results of our LVG analysis of the ortho-NH_3 excitation coupled with our measured $T_B(3, 3) \gtrsim 1127$ K and $\Delta v_{FWZI}(3, 3) \simeq 1.2$ km s^{-1} lead naturally to the conclusion that the westernmost $NH_3(3, 3)$ peak in our maps is the first $NH_3(3, 3)$ maser detected in the interstellar medium.

One of the most interesting properties of the $NH_3(3, 3)$ maser emission is the remarkable similarity between its position and spectral profile and those of the CH_3OH masers (Fig. 1). This similarity can only indicate that the $NH_3(3, 3)$ and CH_3OH masers are produced by the same source. The statistical equilibrium calculations of the CH_3OH excitation presented in Plambeck & Menten (1990) indicate that for simultaneous CH_3OH maser emission to occur in the $4_{-1} \rightarrow 3_0$ E, $7_0 \rightarrow 6_1 A^+$, $5_{-1} \rightarrow 4_0$ E, and $8_0 \rightarrow 7_1 A^+$ transitions, the CH_3OH abundance must be 10^{-7}, the kinetic temperature 100 K, and the H_2 density in the range from 10^4 to 10^6 cm^{-3}. These values for $n(H_2)$ and T_K are consistent with the requirements for the production of $NH_3(3, 3)$ maser emission.

Plambeck & Menten (1990) have suggested that the interaction between outflows and dense gas clumps may lead to the formation of CH_3OH masers. Compact ($\theta_s \lesssim 20''$), broad ($\Delta v \gtrsim 12$ km s^{-1}) wing emission is observed toward the MM 1 position [$\alpha(1950) = 20^h37^m14^s.2$, $\delta(1950) = 42°12'11''$, $V_{LSR} = -4$ km s^{-1}] of DR 21(OH) in CS $J = 5 \rightarrow 4$ (Richardson et al. 1993), CS $J = 7 \rightarrow 6$ (Mangum 1994), and CO $J = 3 \rightarrow 2$ (Mangum 1994) emission. The spatial distribution of this emission is effectively east-west, with blueshift (relative to MM 1) located to the west and redshift located to the east. As the $NH_3(3, 3)$ maser is located within the western (blueshifted) lobe of this outflow, this coincidence suggests that $NH_3(3, 3)$ maser emission may be produced by the interaction between outflows and dense gas condensations.

Recently Bachiller, Martín-Pintado, & Fuente (1993) have shown that $NH_3(3, 3)$ *thermal* emission profiles are similar to SiO emission profiles toward a number of star formation regions. Bachiller et al. (1993) suggest that this similarity indicates that $NH_3(3, 3)$ emission, like SiO emission, arises in shocked material located along jets or collimated outflow lobes. Our $NH_3(3, 3)$ measurements do not have the flux sensitivity necessary to detect any thermal outflow emission. Nonetheless, there appears to be strong evidence for the association of $NH_3(3, 3)$ thermal and maser emission and the outflow emission from star formation regions.

As OH and H_2O masers are observed to be flux variable on timescales as short as several weeks, it might be expected that $NH_3(3, 3)$ maser emission would show variability. Since we found no change in the maser flux between our two independent measurements, the $NH_3(3, 3)$ maser shows no flux variability on timescales less than 1 year. Interestingly, this is consistent with the observation that CH_3OH masers show no flux variability on timescales less than several months (Batrla & Menten 1988).

3.2. *Interstellar Chronography and the* $NH_3(3, 3)$ *Maser*

Flower et al. (1990) have modeled the effects of the evolution of the ortho-H_2/para-H_2 ratio on the production of $NH_3(3, 3)$ maser emission. They point out that differences between the collisional propensity rules for collisions involving the two species of H_2 critically influence the production of $NH_3(3, 3)$ maser emission. Collisional excitation of the (3, 3) inversion doublet by para-H_2 shows a propensity for the upper state in this transition, which can lead to a population inversion in the transition. Collisional excitation by ortho-H_2, on the other hand, shows no propensity for either state and will tend to inhibit population inversion. Flower et al. (1990) found that for $T_K = 50$ K and $n(H_2) \lesssim 10^6$ cm^{-3} population inversion occurs for $n(\text{ortho-}H_2)/n(\text{para-}H_2) \lesssim 1.3$. Since the ortho-$H_2$/para-$H_2$ ratio is expected to evolve with cloud age, time-dependent models of the chemistry in a molecular cloud can be used to predict $n(\text{ortho-}H_2)/n(\text{para-}H_2)$ ratios as a function of cloud age. Using the chemical model of Pineau des Forêts, Roueff, & Flower (1990), Flower et al. (1990) find that for $n(H_2) = 5 \times 10^4$ cm^{-3} and $T_K = 30$ K the cloud age must be less than

10^6 yr. Because the point of conversion at which the gas goes from being mainly ortho-H_2 to one comprised mainly of para-H_2 is rather sharp in these chemical models, changes in T_K and $n(H_2)$ are not likely to have a large influence on this cloud age estimate. Given the observed association between the $NH_3(3, 3)$ maser and outflow emission (§ 3.1), this cloud age estimate might actually represent an upper limit to the age of the outflow.

4. CONCLUSIONS

$NH_3(3, 3)$ maser emission has been discovered toward the DR 21(OH) molecular cloud. The remarkable spatial and spectral coincidence of this ammonia maser with CH_3OH masers indicates that NH_3 and CH_3OH masers require similar sets of physical conditions. Both types of masers, along with thermal $NH_3(3, 3)$ emission, are likely produced within the shocked material associated with molecular outflows. Using the fact that the existence of $NH_3(3, 3)$ maser emission is dependent upon the ortho-H_2/para-H_2 ratio, $NH_3(3, 3)$ maser emission can be used as an interstellar chronometer. Time-dependent chemical models of the ortho-H_2/para-H_2 ratio indicate that the cloud which gives rise to the $NH_3(3, 3)$ maser emission must be less than 10^6 years old.

We thank the staff at the VLA for assistance with the calibration of the data. This work was supported in part by Texas Advanced Research Program grant 003658-285.

REFERENCES

Bachiller, R., Martín-Pintado, J., & Fuente, A. 1993, ApJ, 417, L45
Batrla, W., & Menten, K. M. 1988, ApJ, 329, L117
Blake, G. A., Sutton, E. C., Masson, C. R., & Phillips, T. G. 1987, ApJ, 315, 621
Brown, R. D., & Cragg, D. M. 1987, Australian Physicist, 24, 184
Cesaroni, R., Walmsley, C. M., & Churchwell, E. 1992, A&A, 256, 618
Danby, G., Flower, D. R., Valiron, P., Schilke, P., & Walmsley, C. M. 1988, MNRAS, 235, 229
Flower, D. R., Offer, A., & Schilke, P. 1990, MNRAS, 244, 4P
Gómez, Y., Rodríguez, L. F., Garay, G., & Moran, J. M. 1991, ApJ, 377, 519
Guilloteau, S., Wilson, T. L., Martin, R. N., Batrla, W., & Pauls, T. A. 1983, A&A, 124, 322
Haschick, A. D., & Baan, W. A. 1989, ApJ, 339, 949
Haschick, A. D., Menten, K. M., & Baan, W. A. 1990, ApJ, 354, 556
Hermsen, W., Wilson, T. L., & Bieging, J. H. 1988, A&A, 201, 276
Irvine, W. H., Schloerb, F. P., Hjalmarson, Å., & Herbst, E. 1985, in Protostars and Planets II, ed. D. C. Black & N. S. Matthews (Tucson: Univ. Arizona Press), 579
Johnston, K. J., Stolovy, S. R., Wilson, T. L., Henkel, C., & Mauersberger, R. 1989, ApJ, 343, L41
Madden, S. C., Irvine, W. M., Matthews, H. E., Brown, R. D., & Godfrey, P. D. 1986, ApJ, 300, L79
Mangum, J. G. 1994, in preparation
Mangum, J. G., & Wootten, A. 1994, in preparation
Mangum, J. G., Wootten, A., & Mundy, L. G. 1991, ApJ, 378, 576
———. 1992, ApJ, 388, 467
Mauersberger, R., Henkel, C., & Wilson, T. L. 1987, A&A, 173, 352
Mauersberger, R., Wilson, T. L., & Henkel, C. 1986, A&A, 160, L13
———. 1988, A&A, 201, 123
Norris, R. P., Booth, R. S., Diamond, P. J., & Porter, N. D. 1982, MNRAS, 201, 191
Pineau des Fôrets, G., Roueff, E., & Flower, D. R. 1990, MNRAS, 244, 668
Plambeck, R. L., & Menten, K. A. 1990, ApJ, 364, 555
Richardson, K. J., Sandell, G., Cunningham, C. T., & Davies, S. R. 1993, A&A, in press
Wilson, T. L., Batrla, W., & Pauls, T. A. 1982, A&A, 110, L20
Wilson, T. L., & Henkel, C. 1988, A&A, 206, L26
Wilson, T. L., & Mauersberger, R. 1990, A&A, 239, 305
Woody, D. P., Scott, S. L., Scoville, N. Z., Mundy, L. G., Sargent, A. I., Padin, S., Tinney, C. G., & Wilson, C. D. 1989, ApJ, L41